Categorization and Analysis of Defects in Cryogenic Laser Fusion Targets

Lauren M. Weiss

Brighton High School
Rochester, NY

Adviser: Luke M. Elasky

Laboratory for Laser Energetics
University of Rochester
Rochester, NY
August 2005

Abstract

Laser fusion is a technology under development that will use the fusion of hydrogen isotopes as a power source. It uses laser energy to irradiate a small, cryogenic target containing deuterium ice, causing the deuterium in the target to compress to extreme densities and fuse. In the process of freezing the deuterium, defects can form. This work focused on defects, which are localized nonuniformities in the ice that can hinder fusion reactions. Defects in a variety of targets were catalogued using shadowgraphy, a type of imaging. Categorization was based on the defect's size, shape, depth in the ice layer, and light intensity pattern. Principal defect categories include bumps, cracks, double defects, and ghost rings. The locations of the defects were analyzed to determine whether environmental factors in the layering sphere (the spherical chamber in which the ice layer is formed) were causing the defects. This analysis showed that 1) many bumps and closed cracks occur in diametrically opposite pairs, and 2) the defects known as ghost rings occur in a specific location relative to glue spots (which are used to mount the targets) on one side of the layering sphere, suggesting that the glue spots cause these defects. The glue spots are most likely heated by nearby bright spots in the layering sphere because the defects only occur in a certain region.

1. Introduction

1.1 Cryogenic Targets

To achieve laser fusion, it is necessary to uniformly compress as much deuterium fuel as possible to a very high density. To maximize the amount of fuel, cryogenic targets are used (see Fig. 1a). Cryogenic targets are preferable to room-temperature

targets because solid deuterium is denser than gaseous deuterium, so more deuterium is available for fusion in a cryogenic target.

Cryogenic targets are formed by filling a plastic shell with 1000 atm of deuterium gas and placing it in an apparatus called the layering sphere (see Fig. 1b). The layering sphere is maintained just below the deuterium triple point, which is 18.73 K. When the target has frozen, mid-infrared irradiation bounces around the inside of the layering sphere to heat the target uniformly. Because thick regions of ice absorb more IR radiation, the deuterium in these regions heats up, sublimes, and then condenses in colder regions of the target. This continues until the deuterium ice layer achieves thermal equilibrium, a condition that theoretically results in a uniform ice layer.[1]

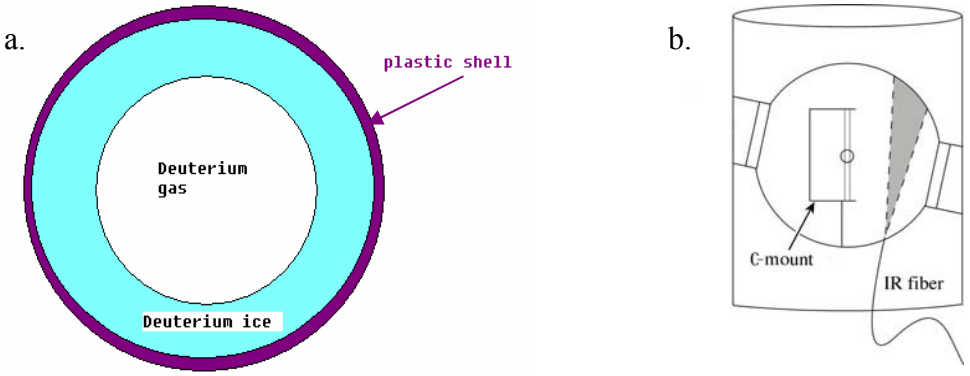

Figure 1. (**a**) Cross-section of a cryogenic target. The diameter of the target is ~900 μm, the ice is ~100 μm thick, and the plastic shell is 3 μm thick. (**b**) A cross-section of the layering sphere. The tiny circle in the center is the target, which is suspended from four strands of spider silk which are attached to a C-mount. The IR fiber provides internal heating to create a uniform temperature within the layering sphere.

In order for fusion reactions to occur, the target must compress uniformly. By Newton's Law, F=ma, the pressure from the plasma formed by laser irradiation on the target's plastic shell will accelerate thin regions of ice toward the target's center faster than thick regions, because thin regions are less massive. Efficient fusion relies on as much fuel as possible reaching the center of the target simultaneously, so any time lag

decreases the amount of fuel available for fusion and the maximum compression that can be achieved, and thus the number of fusion reactions. Therefore, the ice layer must be uniform to maximize energy output.

There are two general types of nonuniformity in the ice layer. One is an asymmetry, in which the change of the ice thickness around the target is gradual, like a slope in a road. The other is a defect, which is a localized nonuniformity in the ice layer, like a pothole. Although past research has studied asymmetries[2,3], little work has been done to analyze defects because of their complexity. To understand why defects are relatively difficult to interpret, one must understand shadowgraphy.

1.2 Shadowgraphy

Targets are characterized using shadowgraphy, an imaging process that involves backlighting the target to produce an image (see Fig. 2). Collimated light starts behind the target, travels through the target, is collected by a lens in front of the target, and is imaged onto a CCD. Light that is collected in the optics appears to come from the plane through the target's center (the object plane), so the light intensity patterns in the image correspond to the light intensity patterns in that plane. Light intensity is scaled from black to white, with black corresponding to no light in that area of the object plane, and white corresponding to very high intensity light.

Two types of rays are collected: A-rays and B-rays. A-rays pass through a large central region of the target, whereas B-rays refract off the inner ice surface. When the paths of B-rays are traced back to the object plane, they appear to come from a narrow

region known as the "bright ring." A defect can alter or obstruct either type of ray, as illustrated in Fig. 2b.

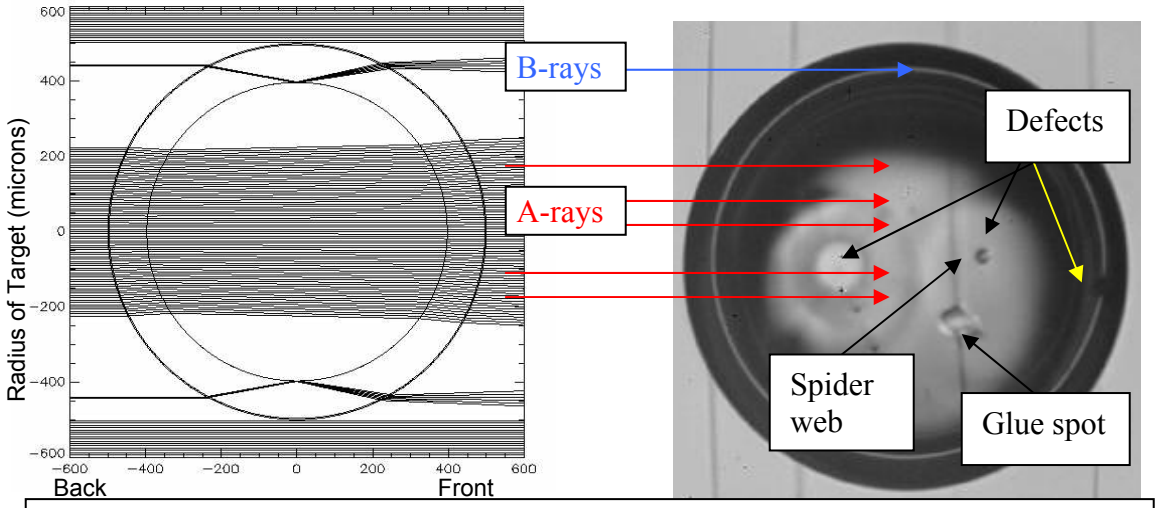

Figure 2. (**a**) Side view of the target showing light rays traveling from the back of the target to the front. A-rays pass through the center of the target; B-rays bounce once off the inner ice surface. The window scale is from -600 to 600 µm. (**b**) A typical shadowgram. The outermost black circle is a silhouette of the target. The spider web and glue spots that suspend the target are visible. The light central area of the shadowgram is from the A-rays and shows two circular defects. The thin white ring near the edge of the target is the bright ring produced by the B-rays and also indicates a defect.

To understand what causes defects, it is necessary to know where they form. Therefore, the defect's origin is mapped with respect to a coordinate system embedded in the target using standard spherical coordinates, with θ measuring the angle from the vertical z-axis and Φ measuring the angle about the z-axis.

In order to find and categorize all of the defects on a target, multiple shadowgrams are taken from different angles by rotating the target about its vertical axis. Each target is viewed by two cameras, at θ = 78° and 63°, which take 25 images each. This creates a shadowgram for every 15° of rotation in each camera's image set.

1.3 Defect Categorization

Scientists have studied cryogenic targets extensively using the bright ring to analyze ice surface nonuniformities and simulated defects.[2,3,4] Although defects have always been visible in the A-rays, no work had been done to understand their nature because there was no way to determine the depths of defects in the ice layer until a program known as Liger was developed.[5] Liger enables the depth of a defect to be calculated, making it possible to include this information in the characterization of defects. In Ref. 5, Liger was used to characterize a single defect in a single target.

This work used Liger and my own observations to systematically investigate defects. Twenty-six defects in eleven targets were analyzed. Many defects had similar physical properties. These defects were categorized. The most important factors in categorizing a defect were the defect's shape, size, light intensity pattern, depth in the ice, and the changes produced in the bright ring when the defect was on the side of the target.

Most of the defects that were examined were categorized as bumps, open cracks, closed cracks, ghost rings, or double defects, all of which are discussed in detail in the following sections.

2. Bumps

2.1 Observations

Bumps are the round, smooth defects pictured in Fig. 3. Bumps usually range from 150 to 200 microns in diameter. They appear gray on the front of the target and white on the back. This allows us to conclude that they are convex structures on the inner ice surface, as explained in Section 2.2.

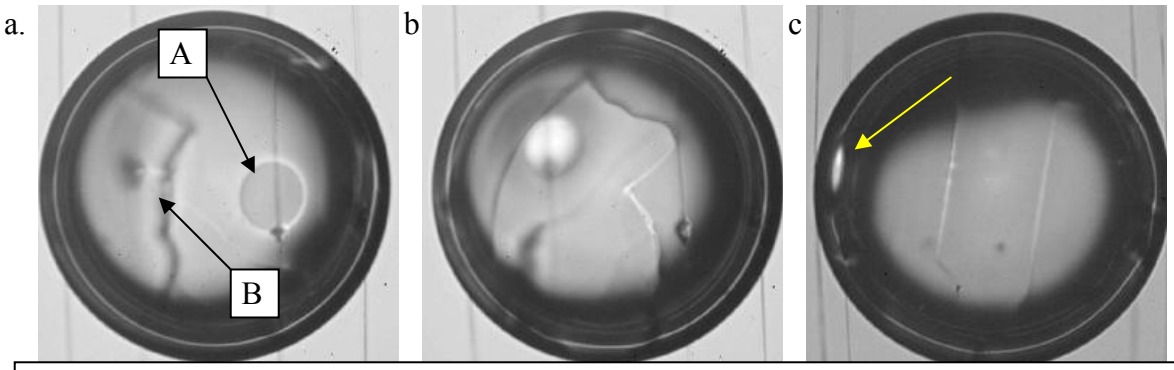

Figure 3. Three views of a target containing a circular defect (a bump) [A] and an open crack [B]. (**a**) On the front of the target, the bump is a gray spot surrounded by a thin white ring. (**b**) On the back of the target, the bump is a white spot surrounded by a thin gray ring. (**c**) The bump forms a rice-grain shaped region of high-intensity light in the bright ring (indicated by the arrow) when the bump is on the left side of the target. Target: Cryo-2041-315; Shadowgram sets: 2x16817, 2y16817; Date: 2004-04.

2.2 Liger Analysis

Liger uses both A-rays and B-rays to approximate the depth of a defect in the ice. Liger displays 50 shadowgrams in sequence. A user examines each shadowgram and flags points around the perimeter of the defect to form a polygon (see Fig. 4). The program establishes a grid of pixels in the central region of the shadowgram. The user clicks once in the area that is not part of the defect, marking the rays that go through it as "good" A-rays. The user also flags the abnormal arcs in the bright ring. The paths that these rays would have followed if they were not blocked are known as "bad" B-rays.

Figure 4. User's selection of good A-rays and bad B-rays from Fig. 3a. The user flags points indicated by the circles; the white dots represent the good A-rays (although the program traces more rays than those shown).

Liger calculates the paths of the good A-rays and bad B-rays and stores the paths in a 3-D matrix. By counting the number of rays that pass through each cell, Liger constructs a 3-D model of the target. The user views the model in horizontal slices similar to those of a CAT scan. A Liger analysis of a bump defect is shown in Fig. 5. The intensity is scaled so that cells that contain only good A-rays are white, cells that contain zero good A-rays are black, and cells that contain some good A-rays are shades of gray. The defect lies within the black area in the upper left of Fig. 5a. However, it could be at any depth within this area.

To indicate the depth of the defect, Liger incorporates the paths of the bad B-rays into the 3-D model. The intersection of bad B-rays with cells that contained zero good A-rays is shown in Fig. 5b. This intersection maps the approximate depth of the defect because the B-rays and A-rays that were blocked followed different paths through the ice. Figure 5b indicates that the defect is on the inner ice surface.

a. b.

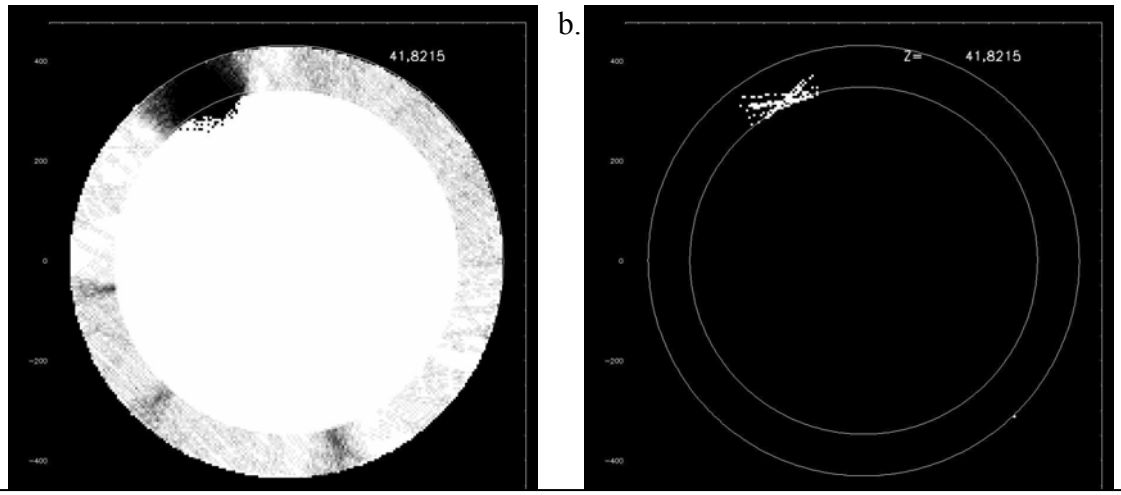

Figure 5. (**a**) Liger analysis of a bump defect using only A-rays, in the plane z = 42 μm. The white areas correspond to the paths of good A-rays. The dark region near the upper left indicates the general location of the defect. (**b**) Analysis including B-rays, showing the intersection of the dark region of (a) and the bad B-rays. This narrows the possible region in which the defect could be. The window scale is from -400 to 400 μm.

Although it can locate a defect, Liger cannot determine whether the defect is a concave region, a convex region, or a region that contains impurities; it merely shows that the region blocked or scattered light. Yet, we can determine whether a round defect is convex or concave based on its light intensity pattern,[6] as indicated in Fig. 6.

When light goes through convex defects on the back, it is refracted inwards, as indicated in Fig. 6a. The apparent area of the defect is smaller than its true area, and so the defect appears brighter. A narrow region of low-intensity light surrounds the defect because the rays that ordinarily would have gone through this area went through the small, bright region instead. The resulting shadowgram is seen in Fig. 3b. When the convex defect is viewed on the front, the refracted rays projected back to the object plane appear to come from a larger area, and so the defect appears darker. A narrow region of high-intensity light surrounds the defect because the rays that extend beyond the true area of the defect enter regions that already contain rays, thus increasing the concentration of rays there (see Fig. 3a). Concave defects disperse light, and so they create the reverse of the convex patterns. Ray-traces similar to those shown in Fig. 6 indicate that a bump that is 3 μm high produces an intensity pattern similar to those of typical bump defects.[7]

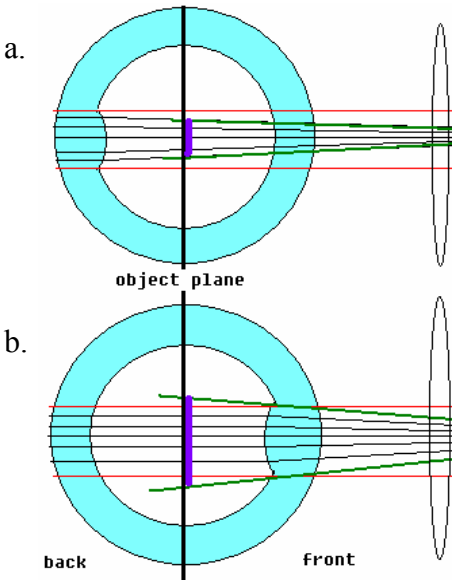

Figure 6. Side view of ray paths through a bump. (**a**) Light from the back of the target is refracted by the bump. As the green rays indicate, it passes through an area on the object plane (indicated in purple) that is smaller than the true area of the defect. (**b**) Light that passes through a convex defect on the front of the target appears to come from an area larger than the true area of the defect when it is projected back to the object plane.

3. Open Cracks

3.1 Observations

Open cracks are long and narrow, as shown in Fig. 3. They are narrower than 20 microns and longer than 200 microns. Although we cannot determine the concavity of open cracks, we assume that they are cracks because the ice contracts when the target is cooled to ~1K below its triple point.

Because open cracks are so narrow, they cause limited interference to the rays that form the bright ring. Cracks that run mostly vertically, like the one in Fig. 3, will make large voids in the bright ring, but only when they are lined up exactly on the side of the target. Cracks that run horizontally will only make a small break in the bright ring, but this break will show up at more angles of target rotation.

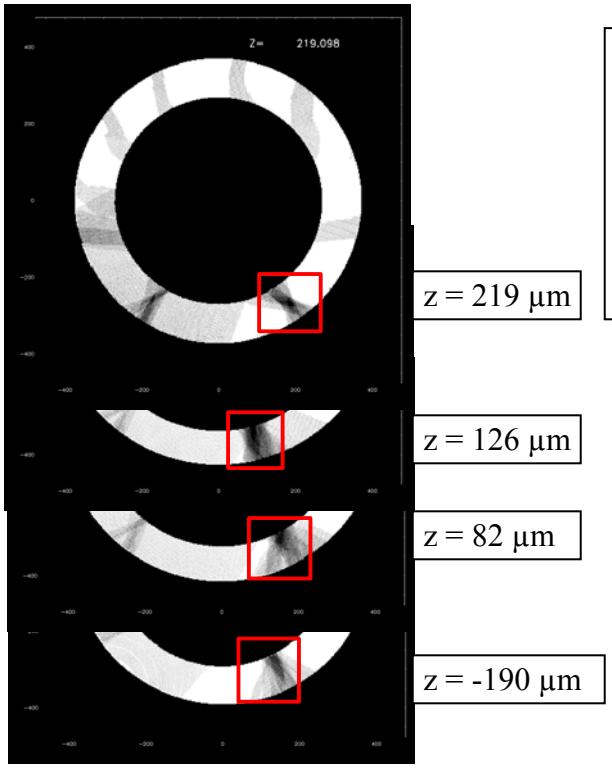

Figure 7. Liger analysis of the open crack shown in Fig. 3. Slices are taken at different heights in the target. The red boxes indicate portions of the crack discussed in the text. Cryo-2041-315, 2y16817, 2004-04.

3.2 Liger Analysis

A Liger analysis of the open crack in the target of Fig. 3 is shown in Fig. 7. Because open cracks have limited impact on the bright ring, they are difficult to identify in the B-rays of a target. However, they are narrow enough that the combination of A-rays from different angles can resolve their depth. This can be seen in the bottom three slices of Fig. 7, in which the black regions taper as their distance from the inner ice layer increases. This indicates that the open crack occurs near the inner ice surface. Also, only a defect on the inner surface could leave the light gray shadows that fan out from the inner ice surface. These shadows occur because the defect prevents A-rays from passing through the normal ice at certain angles.

4. Closed Cracks

4.1 Observations

Closed cracks are complex cracks of polygonal structure that are generally from 100 to 400 microns in diameter. One example of a closed crack is shown in Fig. 8. Of all the defects, closed cracks vary the most in appearance; no two have the same shape. Every closed crack encountered in this work was opposite a bump, although only three of five targets that had a bump had a closed crack opposite the bump.

The Liger analysis of a closed crack is very similar to that of a bump, so it is not shown. The intersection of A-rays and B-rays shows that closed cracks are located on the inner ice surface. Liger also shows that the bump and closed crack are ~180 degrees apart, as illustrated in Fig. 8b.

a. b.

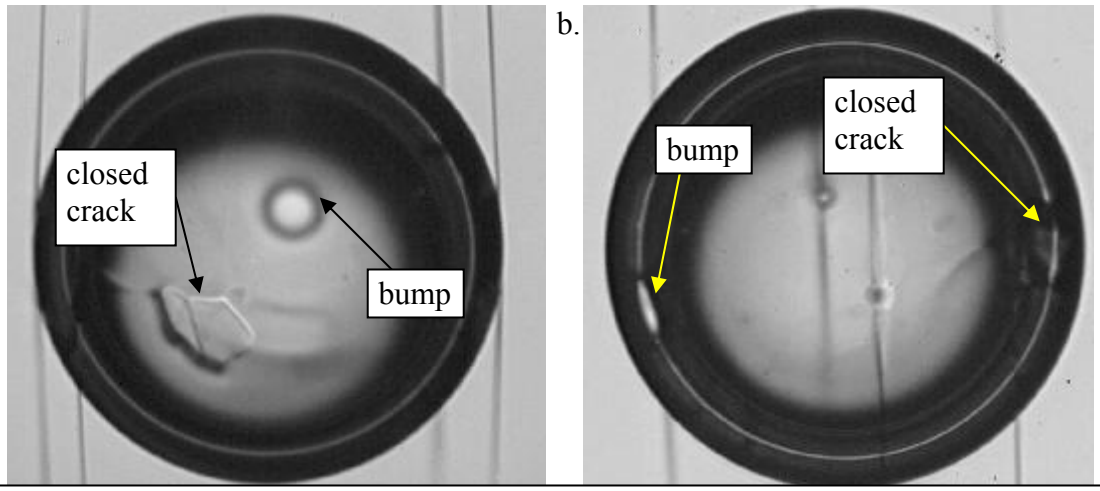

Figure 8. (**a**) A polygonal closed crack on the front of the target, viewed at Φ=340°. The closed crack is opposite a bump on the back. (**b**) The same target, with the closed crack on the right and the bump on the left, viewed at Φ=241°. The bump produces the rice-grain of light in the bright ring on the left, and the closed crack produces the void and blemish in the bright ring on the right. Cryo-2039-313; 2x15832, 2y15832; 2004-04.

4.2 Possible Explanation

The diametrically opposite positioning of the bump and the closed crack might be a result of how the deuterium ice layer is formed. To form the ice layer, the target is cooled in such a way that the liquid deuterium first crystallizes at a single point. Crystallization continues from the seed and expands around the surface of the target.

One place where a defect could form is the location of the seed crystal. Because the target would be colder there, the ice would form a thicker layer. This might cause a bump in the ice. Since the crystal surface must eventually reconvene at the polar opposite point from the seed crystal, another defect could form at the point of convergence as the crystal fronts come together. The closed crack possibly forms this way because it appears to have a crystalline structure, and it often appears to contain several overlapping features.

5. Ghost Rings

5.1 Observations

Ghost rings are halo-like regions that are usually centered on the glue spots used to mount the target, as shown in Fig. 9a. There are four glue spots on each target, positioned equidistantly around the equator. Ghost rings only form around or near large glue spots (~50 μm in diameter) in a certain region of the layering sphere. This region is along the equator between approximately $\Phi = 250°$ and 300°.

The curvature of the ghost ring is very subtle because it does not create a break or void in the bright ring; it only produces a slight ripple, as shown in Fig. 9b. This perturbation is too subtle and gradual for Liger to analyze. Therefore, Liger cannot characterize ghost rings effectively.

Ghost rings on the front are dark with a white interior (see Fig. 9a), and on the back they are white with a dark interior.

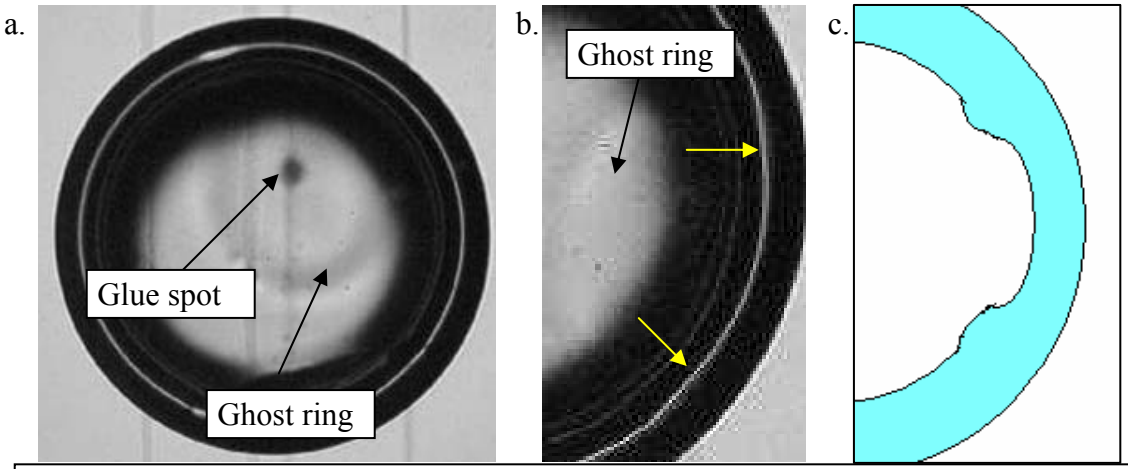

Figure 9. (**a**) A ghost ring on the front of the target. The ring is dark with a bright interior. The dark spot is a glue spot. (**b**) Perturbations in the bright ring caused by the ghost ring indicated with yellow arrows. (**c**) Proposed cross-section through a ghost ring (exaggerated).

5.2 Proposed Explanation

Ghost rings appear to be formed by the glue spots at their centers. According to this model, the glue spot absorbs energy from the IR radiation and dissipates it as heat through the ice layer by conduction and thus creates a hot spot on the inner ice surface. The extra heat causes the deuterium atoms on the inner ice surface to sublimate, creating thinner ice in the region of the hot spot.[1] When the displaced deuterium atoms encounter sufficiently cold ice, they condense, forming a thick ring of ice around the hot spot.

We can infer the thickness of the ice in a target based on the radius of the bright ring.[3] Thick ice creates a small radius, whereas thin ice creates a large radius. From the variations in bright-ring radius, we can postulate a cross-section of the ghost ring (see Fig. 9c). This suggests that the ghost ring is a region of thin ice surrounded by a region of thick ice, where the thin ice is the hot spot in the middle and the thick ice is the ring.

The only glue spots that produce ghost rings are large (50 μm in diameter) and are located between $\Phi = 250°$ and 300°. Why do ghost rings only form around these types of glue spots? A large glue spot would create a more pronounced hot region than a small glue spot because a large glue spot would absorb more IR radiation. The location of the glue spot during target freezing affects whether a ghost ring will form because the distribution of IR radiation inside the layering sphere is not completely uniform. A region of the layering sphere at $\Phi \approx 285°$ is much brighter than the rest of the layering sphere. This is because the injected IR light from the short optical fiber makes its first bounce at that location[8] (see Fig.10). Because the initial bounce is significantly brighter than other bounces, the target receives more illumination from this angle than any other angle. Therefore, a hot spot is formed on the side of the target nearest this incident

radiation. If a large glue spot is in the vicinity of the hot spot, it will absorb some of the excess radiative energy and form a ghost ring. However, the hot spot would not affect the ice in the absence of a glue spot because the ice only absorbs ~10% of the IR light, whereas the glue spot absorbs nearly all of it.

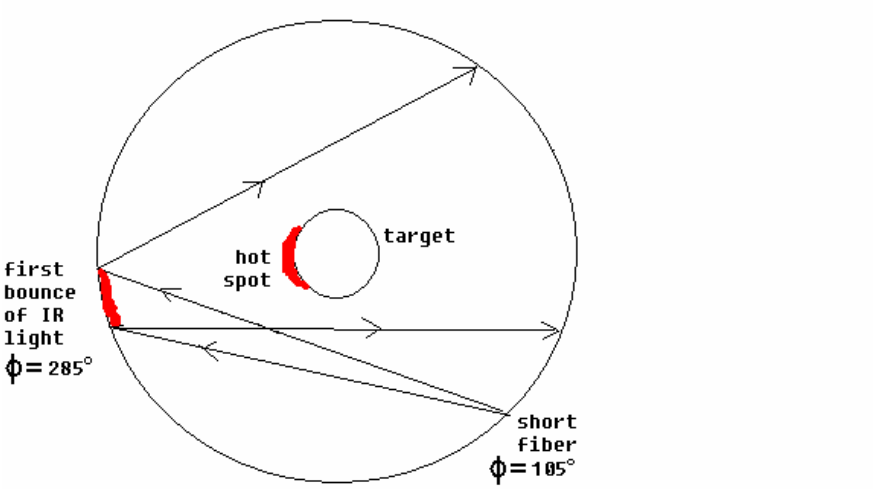

Figure 10. Schematic cross-sectional side view of the layering sphere. The short fiber at Φ=105° illuminates the inside of the sphere with mid-IR radiation. The light first bounces off the inside of the sphere at Φ = 285°, resulting in the target being preferentially heated to form the hot spot shown.

6. Double Defects

Double defects appear to be two mutually concentric defects, as shown in Figure 11. The key elements of the double defect are an inner defect of about 100-150 microns in diameter, which resembles a bump in the shadowgrams, and an outer defect of about 300-350 microns in diameter that surrounds it. On the front of the target, double defects have a gray inner defect, and the outer defect is barely visible (see Fig. 11a). On the back, double defects have a white inner defect, and the outer defect is easily visible as a dark ring (see Fig. 11b). Because the inner defect is bright on the back, it is a convex feature.

a. b.

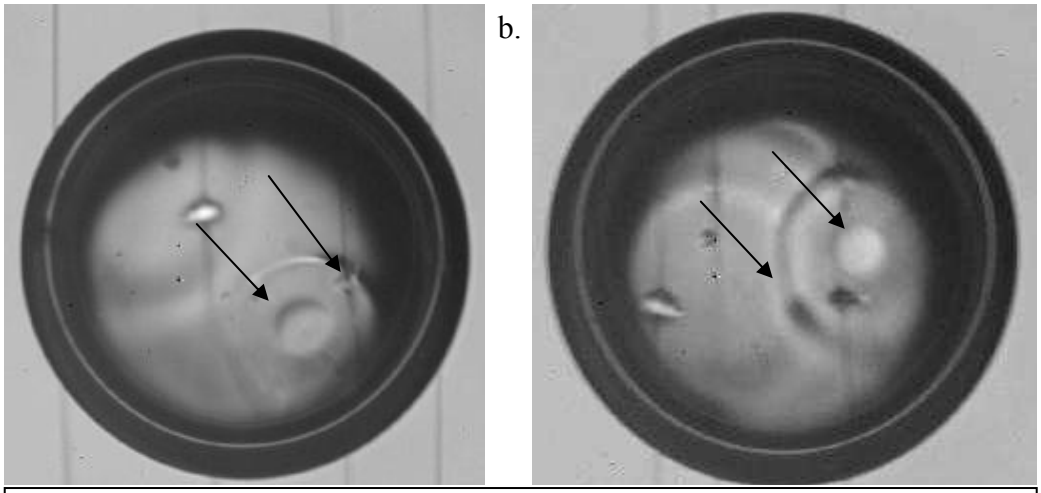

Figure 11. Two views of a double defect. (**a**) Double defect on the front of the target, with the inner and outer defects indicated with arrows. (**b**) The same double defect on the back of the target, with a bright inner area and a dark outer ring. Cryo-2036-344, 1y18730, 2004-07.

6.2 Liger Analysis

Several attempts were made to analyze double defects with Liger. An example for a target similar to that shown in Fig. 11 is shown in Fig. 12. The A-rays helped determine the size of the inner and outer defects (see Fig. 12a). However, analyses including the B-rays did not display believable depths for the inner defect. Fig. 12b shows an inner defect that appears to extend through the entire volume of the ice. However, as illustrated by the blue ray path in Fig. 12b, the apparent depth of the inner defect is probably a result of bad B-ray paths from the outer defect intersecting the inner dark region of Fig. 12a. Thus, B-rays that were blocked by the outer defect appear to have been blocked by the inner defect also. This interference of the outer defect makes it impossible for Liger to accurately characterize double defects. Because Liger and the shadowgrams do not provide sufficient information about double defects, no explanation for their origin has been proposed.

a. b.

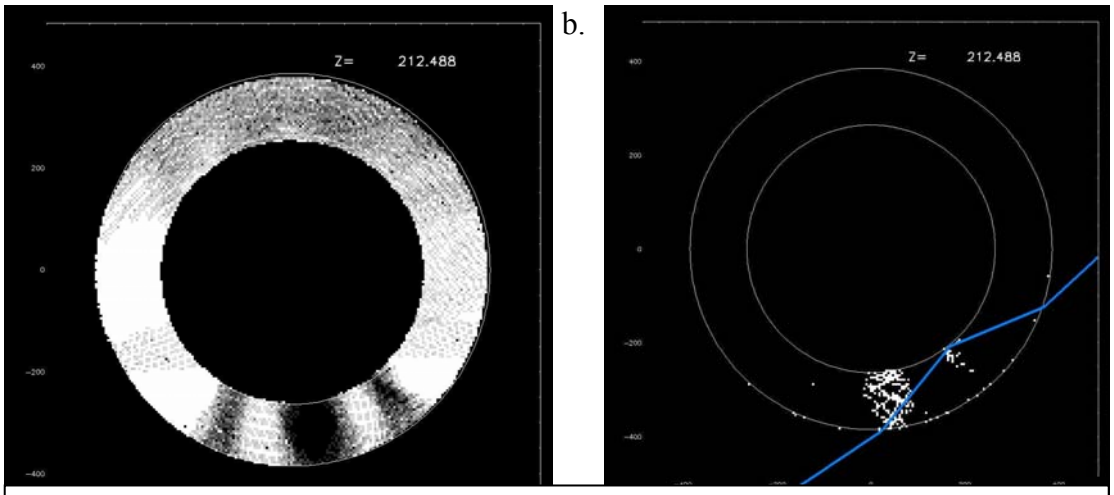

Figure 12. Liger analysis of a defect similar to that of Fig. 11, in the plane z = 212 µm. (**a**) Analysis based on the A-rays alone, showing the double defect but providing no depth information. (**b**) Intersection of paths of bad B-rays and the dark area of (a), showing an inner defect of about 100 µm in diameter that appears to extend through the full volume of the ice, surrounded by a thin, ring-shaped outer defect of about 350 µm in diameter that occurs on the inner ice surface. The blue ray path illustrates how B-rays blocked by the outer defect could appear to be blocked by the inner defect. Cryo-2044-302, 2x15633, 2y15633, 2004-04.

Because of its limitations, Liger proposes the cross-section of a double defect similar to that of Fig 13a. However, an analysis based on the light intensity pattern of the defect yields a proposed cross-section that is shown in Figure 13b.

a. b.

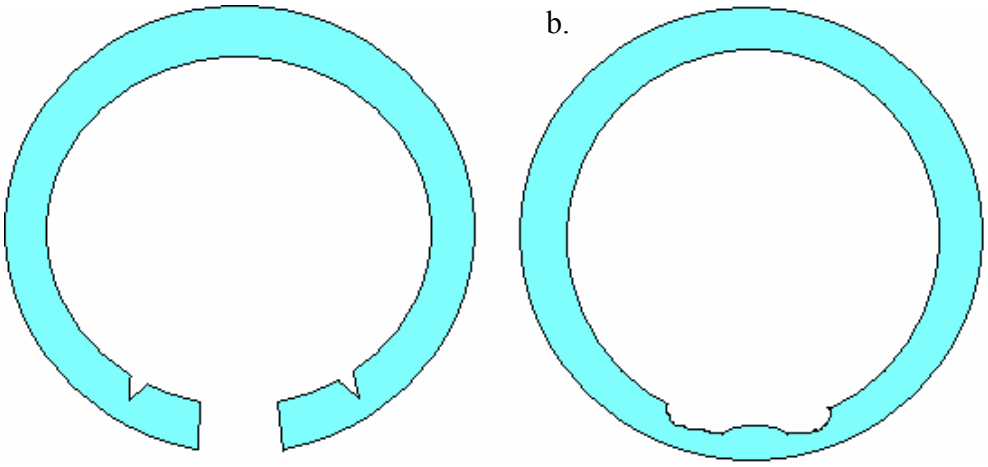

Figure 13. (**a**) Cross-section through a double defect based on Liger analysis. (**b**) A more likely cross-section through the defect (exaggerated).

7. Summary and Conclusion

In this work, defects in cryogenic targets used for laser fusion research were categorized based on their shape, size, light intensity pattern, depth in the ice, and the fluctuations they produced in the bright ring. Many defects display similar physical properties and are thus easily categorized. The principal categories of defects are bumps, open cracks, closed cracks, ghost rings, and double defects. The results of observations of these defects are summarized in Table 1.

Defect Type	Shape	Diameter (μm)	Concavity	Location	Explanation
Bump	circular	100-200	convex	inner ice surface	coldest spot in crystal formation
Open crack	long and narrow	>200 x <20	concave	inner ice surface	contraction and splitting of cold ice
Closed crack	polygonal	100-400	?	inner ice surface	overlapping crystals
Ghost ring	ring	300-400 (ring ~50 thick)	concave interior, convex ring	inner ice surface, $250^{o}<\Phi<300^{o}$	sublimation by hot glue spot
Double defect	concentric circles	300-350 (inner 100-150)	convex interior	inner ice surface	??

Table 1. Physical properties of common defects and proposed explanations.

All of the observations in this report were made using only eleven targets and twenty-six defects. Except for the double defect, explanations were proposed for how each type of defect formed. It is vital to continue taking shadowgraphs of targets so that more targets can be characterized to test the validity of these explanations.

The only type of defect that is found to correlate with a particular region of the layering sphere is the ghost ring. All of the other defects are distributed randomly.

Bumps and cracks frequently lie on diametrically opposite points on the target. Bumps are possibly formed where a single point on the target is cooled to begin crystallization, and closed cracks could form where the crystal fronts reconvene on the

opposite side and overlap. To determine if a relationship exists between the defects' positions and the point from which the seed crystal is formed, bumps and closed cracks occurring in diametrically opposite pairs must be further examined, especially during the early stages of the freezing process.

Open cracks probably form when the target is ~1K colder than its triple point, causing the deuterium ice to contract.

Ghost rings are almost certainly formed by conductive heating from large glue spots at their center, which absorb extra IR radiation from a bright spot in the layering sphere at $\Phi \approx 285°$. To prevent ghost rings from forming, smaller glue spots should be used, as they would absorb less IR energy.

By understanding how defects form, we can take measures to prevent them by altering the process for manufacturing cryogenic targets. By eliminating defects, we can make the fusion process more energy efficient.

8. Acknowledgements

I would like to thank Mr. Elasky for supervising and guiding my project and for introducing me to the wonders of the cryogenics laboratory. I would also like to thank Dr. Craxton for selecting me to participate in the High School Summer Research program at the Laboratory for Laser Energetics and for taking personal interest in my work. I would also like to thank the other students and staff at LLE for making my summer enjoyable.

9. References

[1] D.N. Bittner et al., *Forming Uniform HD Layers in Shells Using Infrared Radiation,* Fusion Technology **35**, 244-249 (1999).

[2] J.A. Koch et al., *Numerical Raytrace Verification of Optical Diagnostics of Ice Surface Roughness for Inertial Confinement Fusion Experiments,* Fusion Science and Technology **43**, 55-66 (2003).

[3] J.A. Koch et al. *Quantitative Analysis of Backlit Shadowgraphy as a Diagnostic of Hydrogen Ice Surface Quality in ICF Capsules,* Fusion Technology **38**, 123-131 (2000).

[4] J. Sater, D. Bittner. *Shadowgraphy and Spherical Capsules,* General Atomics Report GA-A23240 **5**, 5-12 (1999).

[5] Brewington, Bruce. *3-D Characterization of Deuterium Ice-Layer Imperfections in Cryogenic Inertial Confinement Fusion Targets,* 2004 Summer High School Research Program for High School Juniors, Laboratory for Laser Energetics **337** (March 2005).

[6] Edgell, Dana, Laboratory for Laser Energetics, personal communication (2005).

[7] Brewington, Bruce, *Computer Simulation of Shadowgraphy,* unpublished report, Laboratory for Laser Energetics (2005).

[8] Elasky, Luke, Laboratory for Laser Energetics, personal communication (2005).